Polyhedron 169 (2019) 219–227

Contents lists available at ScienceDirect

Polyhedron

journal homepage: www.elsevier.com/locate/poly

Bis(β-ketoiminate) dioxo tungsten(VI) complexes as precursors for growth of WO_x by aerosol-assisted chemical vapor deposition

Xiaoming Su, Persi Panariti, Khalil A. Abboud, Lisa McElwee-White *

Department of Chemistry, University of Florida, Gainesville, FL 32611-7200, USA

ARTICLE INFO

Article history:
Received 17 March 2019
Accepted 7 May 2019
Available online 16 May 2019

Keywords:
Tungsten oxide
Aerosol-assisted chemical vapor deposition
Single source precursors
Metal oxo complexes
Metal oxide films

ABSTRACT

Bis(β-ketoiminate) dioxo tungsten(VI) complexes WO_2L_2 (L = acNac, $acNac^{Me}$, $acNac^{Et}$) have been synthesized and characterized. The thermal behaviors and possible decomposition mechanisms of these dioxo compounds were studied by TGA, MS and thermolysis. The performance of $WO_2(acNac^{Me})_2$ as an AACVD precursor was evaluated at growth temperatures of 250–550 °C using nitrogen as the carrier gas. The elemental compositions of the as-deposited and sputtered tungsten oxide films were determined by XPS. The morphology and stoichiometry of the as-deposited films were studied by SEM and XRD.

1. Introduction

In recent years, much attention has been given to transition metal oxides (TMOs) as a result of their unique structural, physical and chemical properties. Tungsten oxide (WO_x) is one of the technically appealing multifunctional TMOs with a broad variety of stoichiometries, structures and morphologies depending on processing methods and conditions, which enables applications in various fields such as electrochromic devices [1,2] and organic electronics [3]. The compositional diversity of WO_x originates from the existence of various Magnéli phases ($2.625 \leq x \leq 2.92$, e.g., $W_{32}O_{84}$, W_3O_8, $W_{18}O_{49}$, $W_{20}O_{58}$, and $W_{25}O_{73}$) as well as the ease of generating oxygen defects [4]. Besides chemical composition, features such as crystalline phases, crystallinity and nanostructures can all affect the properties of the material [5,6].

Chemical vapor deposition (CVD) is a process of depositing solid materials by chemical reaction of precursors near or on the substrate surface. This bottom up fabrication method not only can deliver large-scale conformal coatings even on patterned substrates, but also provides the possibility of controlling composition, doping and morphology [7–9]. Use of traditional CVD volatilization techniques such as bubblers requires the precursors to have sufficiently high vapor pressures for efficient delivery. In contrast, aerosol-assisted chemical vapor deposition (AACVD), in which precursor solutions are volatilized as an aerosol generated by an ultrasonic transducer, does not have stringent precursor volatility requirements and thus allows more flexibility in precursor design [10]. In this work we explore the use of nonvolatile tungsten oxo complexes to grow WO_x by AACVD.

Single source metal–organic CVD (MOCVD) precursors for the growth of tungsten oxide include both homoleptic and heteroleptic complexes. Homoleptic precursors are typically alkoxides or aryloxides, e.g., $W(OEt)_5$ and $W(OC_6H_3F_2\text{-}3,4)_6$, which can be either fluorinated or nonfluorinated [8,11]. There is a wider range of heteroleptic candidates that contain various ligands such as oxo, aminoalkoxide, alkoxide and β-diketonate. The incorporation of oxo groups into the tungsten complex takes advantage of existing strong metal–oxygen bonds, which reduces the need for bond cleavage steps and facilitates the precursor decomposition process during material growth. Monooxo complexes of the type $WO(OR)_4$ (R = alkyl) and $WO(OR)_3L$ (R = alkyl, L = aminoalkoxide, β-diketonate/β-ketoesterate, β-ketoiminate/β-iminoesterate) have been characterized and examined as MOCVD precursors; while the study of dioxo tungsten CVD precursors is more limited [12–18]. Due to the interest in the N,O-chelating β-ketoiminate/β-iminoesterate ligands, which have tunable steric and electronic properties, we have reported use of the tungsten oxo complexes $WO(OR)_3L$ (R = alkyl; L = β-ketoiminate/iminoesterate) as AACVD precursors for the growth of WO_x [15]. Probable decomposition mechanisms for these monooxo complexes were proposed but it is not known whether analogous well-defined decomposition channels are available for bis(β-ketoiminate) dioxo tungsten complexes. Herein, we report the synthesis and characterization of tungsten dioxo complexes $WO_2(acNac)_2$ (**1**), $WO_2(acNac^{Me})_2$ (**2**) and $WO_2(acNac^{Et})_2$ (**3**) as well as a demonstration of AACVD growth of tungsten oxide from **2**.

* Corresponding author.
E-mail address: lmwhite@chem.ufl.edu (L. McElwee-White).

https://doi.org/10.1016/j.poly.2019.05.013
0277-5387/

2. Experimental

2.1. General considerations

Methylene chloride, hexane and toluene (Fisher Scientific) were purified using an MBraun MB-SP solvent purification system and stored over activated 3 Å molecular sieves. Diethyl ether and tetrahydrofuran were dried using sodium/benzophenone, distilled, and stored over activated 3 Å molecular sieves before use. Hexamethyldisiloxane, methanol, chloroform-d_1 (Cambridge Isotopes) and benzene-d_6 (Cambridge Isotopes) were stored over 4 Å molecular sieves. Triethylamine was distilled over potassium hydroxide and stored over 4 Å molecular sieves. The compounds $WOCl_4$ [19], WO_2Cl_2(dme) [20], acNacH [21], acNac^{Me}H [22] and acNac^{Et}H [23] were synthesized according to literature procedures. All other solvents and reagents were of analytical grade and were used as received. NMR spectra were recorded on a Varian INOVA 500 spectrometer using residual protons from deuterated solvents for reference. Thermogravimetric analysis was run using a TA Q5000 under nitrogen at a temperature scan rate of 10 °C/min to 600 °C. Mass spectrometry was performed on an Agilent Technologies 6210 Time of Flight instrument using direct analysis in real time. Elemental analyses were performed by Robertson Microlit Laboratories (Ledgewood, NJ).

2.2. Synthesis

2.2.1. WO_2{HC[MeC(O)][MeC(NH)]}$_2$ (**1**)

In the glovebox, 1.01 g (2.68 mmol) WO_2Cl_2(dme) was suspended in 40 mL THF in a Schlenk flask. Then NEt_3 (1.80 mL, 5 eq.) was mixed with 0.532 g (5.37 mmol) acNacH, and 10 mL THF, which was transferred to an addition funnel. The funnel was attached to the Schlenk flask and transferred to the Schlenk line. The WO_2Cl_2(dme)/THF mixture was cooled in a dry ice/acetone bath. The ligand/NEt_3 solution was added to the flask dropwise. The resulting mixture was then left to warm to room temperature and stir for 12 h. Volatiles were removed under vacuum and the flask was transferred to the glovebox. The product was extracted with THF and filtered through Celite giving a yellow solution. The solvent was removed *in vacuo*. The crude product was washed with hexane. Yellow solid (0.41 g, 37%) was obtained. ^{1}H NMR (500 MHz, 25 °C, $CDCl_3$): δ 7.62 (b, 2H, NH), 5.35 (s, 2H, CHCO), 2.15 (s, 6H, $COCH_3$), 2.05 (s, 6H, CH_3CN). ^{13}C{^{1}H} (500 MHz, 25 °C, $CDCl_3$): δ 185.24 (CO), 172.47 (CN), 102.29 (*C*HCN), 27.03 ($COCH_3$), 25.86 ($CNCH_3$). MS (ESI) *m/z* Calc. for $WO_4C_{10}H_{18}N_2$ $[M+H]^+$: 413.0694. Found: 413.0765. FTIR (solid sample): 933 cm^{-1} (W═O, ν(sym)), 892 cm^{-1} (W═O, ν(asym)).

2.2.2. WO_2{HC[MeC(O)][MeC(NMe)]}$_2$ (**2**)

Compound **2** was synthesized following the same procedure as used for **1**. Starting with 1.00 g (2.65 mmol) WO_2Cl_2(dme) and 0.613 g (5.42 mmol) acNac^{Me}H, yellow solid (0.82 g, 70%) was obtained. ^{1}H NMR (500 MHz, 25 °C, $CDCl_3$): δ 5.52 (s, 2H, CHCO), 3.64 (s, 6H, NCH_3), 2.11 (s, 6H, $COCH_3$), 2.11 (s, 6H, CH_3CN). ^{13}C{^{1}H} (500 MHz, 25 °C, $CDCl_3$): δ 182.27 (*C*O), 173.06 (*C*N), 106.90 (*C*HCN), 45.57 (NCH_3), 25.68 ($COCH_3$), 22.78 ($CNCH_3$). MS (ESI) *m/z* Calcd for $WO_4C_{12}H_{21}N_2$ $[M+H]^+$: 441.1007. Found: 441.1024. *Anal.* Calc. for $WO_4C_{12}H_{20}N_2$: C, 32.75; H, 4.58; N, 6.36. Found: C, 32.46; H, 4.63; N, 6.13%. FTIR (solid sample): 929 cm^{-1} (W═O, ν(sym)), 889 cm^{-1} (W═O, ν(asym)).

2.2.3. WO_2{HC[MeC(O)][MeC(NEt)]}$_2$ (**3**)

Compound **3** was synthesized following the same procedure as used for **1**. Starting with 0.497 g (1.32 mmol) WO_2Cl_2(dme) and 0.338 g (2.65 mmol) acNac^{Et}H, yellow solid (0.16 g, 24%) was obtained. ^{1}H NMR (500 MHz, 25 °C, $CDCl_3$): major isomer A (~90%): δ 5.48 (s, 2H, CHCO), 4.06 (m, 1H, NC*H*H), 3.96 (m, 1H, NC*H*H), 2.16 (s, 6H, $COCH_3$), 2.10 (s, 6H, CH_3CN), 1.35 (t, 6H, NCH_2CH_3, J = 7.1 Hz). Isomer B (~10 %, partial spectrum): δ 5.42 (s, 2H, CHCO), 4.26 (m, 1H, NC*H*H), 2.18 (s, 3H, $COCH_3$), 2.10 (s, 3H, CH_3CN), 1.31 (t, 6H, NCH_2CH_3, J = 7.2 Hz). ^{13}C{^{1}H} (500 MHz, 25 °C, $CDCl_3$) major isomer A: δ 181.74 (CO), 171.93 (CN), 107.04 (*C*HCN), 52.24 (NCH_2CH_3), 25.66 ($COCH_3$), 21.82 ($CNCH_3$), 13.69 (NCH_2CH_3). MS (ESI) *m/z* Calc. for $WO_4C_{12}H_{21}N_2$ $[M+H]^+$: 469.1321. Found: 469.1323. FTIR (solid sample): 929 cm^{-1} (W═O, ν(sym)), 886 cm^{-1} (W═O, ν(asym)).

2.3. Film deposition and characterization

Deposition of WO_x was carried out using a custom-built, vertical cold-wall impinging-jet AACVD reactor [24]. Silicon substrates with native silicon dioxide (Si/SiO_2, n-type, (100)) were cleaned in boiling acetone, methanol and deionized water for 3 min each, and then placed on a SiC covered graphite susceptor in the reaction chamber under vacuum. A 0.025 M solution of **2** in diglyme was prepared and transferred into a 10 mL gastight Hamilton syringe. The precursor solution was introduced into a nebulizer with a quartz plate vibrating at 1.44 MHz by a syringe pump with an injection rate of 4 mL h^{-1}. The generated aerosol was delivered to the reaction chamber with nitrogen (1000 sccm, 99.999% purity, Airgas) carrier gas. During deposition (150 min), the reactor pressure was maintained at 350 Torr and the growth temperature was controlled by a radio frequency (RF) heating system on the susceptor.

Elemental compositions of the deposits were determined using ULVAC-PHI XPS Al Kα radiation. O 1s (530.5 eV) or adventitious C 1s (284.8 eV) was used as an internal standard [13,25]. The XPS spectra of the W 4f core level were deconvoluted with parameters of spin–orbit separation ΔE_P ($4f_{5/2}$–$4f_{7/2}$) = 2.18 eV and the W $4f_{5/2}$-to-W $4f_{7/2}$ peak ratio = 3:4. The crystallinities and morphologies were measured using field emission scanning electron microscopy (FESEM, FEI Nova NanoSEM 430) and X-ray diffraction (XRD, Panalytical X'pert Pro).

2.4. Crystallographic structure determination of **2**

X-ray Intensity data were collected at 100 K on a Bruker **DUO** diffractometer using Mo Kα radiation (λ = 0.71073 Å) and an APEXII CCD area detector. Raw data frames were read by the program SAINT[1] and integrated using 3D profiling algorithms. The resulting data were reduced to produce *hkl* reflections and their intensities and estimated standard deviations. The data were corrected for Lorentz and polarization effects and numerical absorption corrections were applied based on indexed and measured faces.

The structure was solved and refined in *SHELXTL2014* [26], using full-matrix least-squares refinement. The non-H atoms were refined with anisotropic thermal parameters and all of the H atoms were calculated in idealized positions and refined riding on their parent atoms. In the final cycle of refinement, 3477 reflections (of which 3371 are observed with $I > 2\sigma(I)$) were used to refine 178 parameters and the resulting R_1, wR_2 and S (goodness of fit) were 0.95%, 2.29% and 1.073, respectively. The refinement was carried out by minimizing the wR_2 function using F^2 rather than F values. R_1 is calculated to provide a reference to the conventional R value but its function is not minimized.

2.5. Thermolysis studies

The sample (complex **2** or the protonated free ligand acNac^{Me}H) was placed in a 10 mL headspace vial which was heated in the GC

oven at 250 °C for 30 min and then cooled to 35 °C. Once cool, the vial was removed from the oven and placed in a sand bath until sampled. A 100-μL sample of the headspace gases was taken with a gas-tight syringe and injected in split mode for GC/EI-MS. Mass spectrometry was conducted on a ThermoScientific (San Jose, CA) DSQ II using electron ionization (70 eV) and an ion source at 250 °C. Gas chromatography was conducted on a ThermoScientific Trace GC Ultra.

3. Results and discussion

3.1. Precursor design

One of the primary requirements for single source precursors is to incorporate all elements of the desired deposits within the complex. Terminal oxo, alkoxide and other oxygen containing ligands such as β-diketonate and aminoalkoxide are commonly used in designing single source precursors to grow metal oxides [27]. In order to maximize precursor properties, an approach of utilizing heteroleptic ligand sets is widely adopted. The precursor design process can be considered as selecting suitable types of ligands and fine-tuning ligand structures to tailor electronic and steric properties.

Prior studies of $WO(OR)_3L$ (R = ^{t}Bu, Me, L = β-ketoiminate, β-iminoesterate) incorporated terminal oxo, alkoxide and chelating mixed N/O ligands into the precursor [15]. The study of decomposition mechanisms of these complexes indicates that the chelating ligand or a *tert*-butoxide group can be protonated from an adjacent *tert*-butoxide functionality with a loss of *tert*-butanol or HL and isobutylene to generate $WO_2(OR)_2$ or $WO_2(OR)L$ species. Replacing the alkoxides of $WO_2(OR)L$ or $WO_2(OR)_2$ with bidentate ligands gives WO_2L_2 moieties which can be more stable due to their coordinative saturation. Furthermore, the incorporation of the second oxo group reduces the need for bond cleavage during deposition compared with the mono oxo complexes; thus, faster growth rates may be achieved.

Complexes of the type WO_2L_2 (L = bidentate ligands) have been explored in photodeposition of WO_3 (L = acetylacetonate) [28], atomic layer deposition (L = amidinate) of WO_3 [29], and oxygen transfer chemistry (L = 4-aryl-pent-2-enolate) [30]. To the best of our knowledge, this type of precursor has not been studied in depositing tungsten oxide by AACVD. Therefore, WO_2L_2 (L = acNac, $acNac^{Me}$, $acNac^{Et}$) complexes have been synthesized and studied as AACVD precursors for the growth of tungsten oxide.

3.2. Synthesis

Complexes **1**–**3** were successfully synthesized by the reaction of 2 equiv of the appropriate ligand with WO_2Cl_2(dme) in the presence of excess NEt_3 (Fig. 1). The product was extracted with THF and the insoluble triethylamine hydrochloride salt was removed by filtration. Removal of volatiles under vacuum gave the desired product.

In other less successful synthetic efforts, the β-ketoimine was reacted with a strong base such as NaH or $LiNMe_2$ to form the alkali metal salt of the ligand, which was then added to the WO_2Cl_2(dme) solution. The desired dioxo product formed but the yield was very low and the product contained noticeable impurities. It has been reported that lithium salts of the β-ketoimines dimerize easily and the lithium halide is relatively soluble in organic solvents [30,31]. The dimerization of the ligand salt and the relatively good solubility of the byproduct (alkali halide) are not conducive to the formation of the dioxo product, which can result in low yields.

3.3. X-ray crystallographic structure determination of **2**

Single crystals of complex **2** were grown by cooling a concentrated solution of **2** in THF to −3 °C. The crystal refinement data are shown in Table 1 and the selected bond lengths and angles are summarized in Table 2.

The molecular structure (Fig. 2) confirms that $WO_2(acNac^{Me})_2$ is a *cis*-dioxo complex that adopts a significantly distorted octahedral geometry around a W(VI) core coordinated by two bidentate β-ketoiminate ligands. The W=O length is within the expected range for *cis*-$[WO_2]^{2+}$ complexes [32,33]. The two enolate oxygens are *trans* to the terminal oxo groups. In order to minimize the competition for available empty metal d orbitals, a weaker π-donor is favored in the *trans* position of the terminal oxo [34,35]. The two imino nitrogens are bent away from the terminal oxo groups with a relatively small N1—W1—N2 bond angle (161.06(5)°) deviating from the ideal octahedral geometry as a consequence of steric repulsion. It is worth mentioning that the two oxo groups have different effects on the imino group. For a specific imino group in the chelating ligand, the oxo group that is aligned for overlap with the π conjugated system has greater influence than the other oxo functionality that is orthogonal to the π-system. For the imino group containing atom N2, for example, the oxo ligand (W1=O2) aligned with the β-ketoiminate π-system (N2—C8—O4) has a stronger repulsion on it leading to an increased bond angle (O2—W1—N2, 99.63(5)°) compared with the other terminal oxo functionality (O1—W1—N2, 91.68(5)°).

The two chelating β-ketoiminates have the same bite angle of 78.57(4)° (O3—W1—N1 and O2—W1—N2), which is in agreement with related literature [36,37]. Consistent with previous study of the β-ketoiminate ligand in $WO(O^tBu)_3$(acNac), the C1—C2 bond (1.423(2) Å) is ca. 0.5 Å longer than the C2—C3 bond (1.378(2) Å) indicating the enolate instead of the enaminate being the major resonance contributor to the overall complex structure.

3.4. NMR spectroscopy

For octahedral *cis*-dioxo bis-bidentate metal complexes, asymmetric bidentate ligands such as β-ketoiminates allow the formation of three isomeric enantiomer pairs (Fig. 3). For O,O-isomers and N,N-isomers, the two bidentate ligands within one molecule are symmetrical, thus only one set of NMR signals will be shown. For the O,N-isomers, the two chelating ligands are not chemically equivalent, and the corresponding NMR spectra will show two sets of ligand signals with equal intensities. ^{1}H NMR spectra of **1** and **2** only show one set of ligand peaks, indicating the formation of

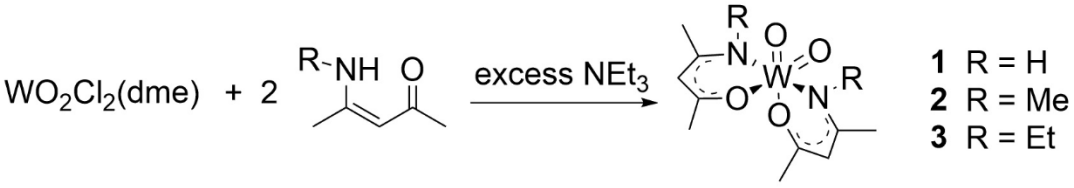

Fig. 1. Synthesis of complexes **1**–**3**.

Table 1
Crystal data and structure refinements for **2**.

Empirical formula	$C_{12}H_{20}N_2O_4W$
Formula weight	440.15
T (K)	100(2)
λ (Å)	0.71073
Crystal system	monoclinic
Space group	$P2_1/n$
Unit cell dimensions	a = 8.1901(3) Å α = 90°
	b = 15.1072(5) Å β = 91.9780(10)°
	c = 11.6076(4) Å γ = 90°
V (Å^3)	1435.35(9)
Z	4
D_{Calc} (Mg m^{-3})	2.037
Absorption coefficient (mm^{-1})	8.059
F(0 0 0)	848
Crystal size (mm)	0.276 × 0.083 × 0.034
θ range for data collection	2.213–28.054°
Index ranges	$-10 \le h \le 10$, $-19 \le k \le 19$, $-15 \le l \le 15$
Reflections collected	30 079
Independent reflections	3477 [R_{int} = 0.0143]
Completeness to θ = 25.000°	100.0%
Absorption correction	none
Refinement method	full-matrix least-squares on F^2
Data/restraints/parameters	3477/0/178
Goodness-of-fit on F^2	1.073
Final R indices [$I > 2\sigma(I)$]	R_1 = 0.0095, wR_2 = 0.0229 [3371]
R indices (all data)	R_1 = 0.0101, wR_2 = 0.0232
Extinction coefficient	n/a
Largest difference peak and hole (e Å^{-3})	0.469 and −0.229

$R_1 = \sum(||Fo| - |Fc||)/\sum|Fo|$, $WR_2 = [\sum[w(Fo^2 - Fc^2)^2]/\sum(w(Fo^2)^2]]^{1/2}$.
$S = [\sum[w(Fo^2)^2 - Fc^2)^2]/(n\text{-}p)]^{1/2}$. $w = 1/[\sigma^2(Fo^2) + (m * p)^2 + n * p]$.
$p = [\max(Fo^2,0) + 2 * Fc^2]/3$, m & n are constants.

Table 2
Selected bond distances (Å) and angles (°) for complex **2**.

Bond parameter		Bond parameter	
W1—O1	1.7323(11)	W1—O2	1.7319(11)
W1—O3	2.1079(10)	W1—O4	2.0971(10)
W1—N1	2.1334(13)	W1—N2	2.1323(13)
C1—C2	1.423(2)	C2—C3	1.378(2)
C8—C9	1.422(2)	C7—C8	1.378(2)
O1—W1—O2	102.38(5)	O1—W1—O4	166.54(5)
O2—W1—O4	89.90(5)	O3—W1—O4	78.57(4)
O1—W1—N1	100.58(5)	O1—W1—N2	91.68(5)
O2—W1—N2	99.63(5)	O2—W1—O3	166.79(5)
O3—W1—N1	80.72(5)	O4—W1—N2	80.72(5)
N1—W1—N2	161.06(5)	O4—W1—N1	84.31(5)

either the O,O-isomer or the N,N-isomer. Considering the fact that the O,O-isomer is favored by the *trans* effect of W=O and the crystallographic study of **2**, it can be inferred that only the O,O-isomer is formed for **1** and **2**.

In case of compound **3**, there are two sets of ligand peaks with different intensities demonstrating the formation of one major symmetric isomer (O,O-isomer or N,N-isomer) and a small amount of the other symmetric isomer. Formation of the N,N-isomer of **3** is probably enabled by the electron repulsion between the substituents on the nitrogen and the oxo groups. The two protons of the methylene group attached to the nitrogen are diastereotopic (H^a and H^b in Fig. 3) and give rise to two different multiplets in the ^{1}H NMR spectrum.

3.5. Thermogravimetric analysis

The TGA analysis of all three complexes **1**–**3** was carried out with the heating rates controlled at 10 °C min^{-1}. The results are shown in Fig. 4. All three compounds show multistep decomposition with an initial major mass loss below 300 °C and a subsequent slow mass loss until 400 °C. With the increased steric bulk of the alkylimino functionality, the onset temperature of fast decomposition slightly decreases and the initial rate of mass loss slightly increases, suggesting more facile reactivity induced by larger alkylimino groups. The TGA residual masses of all three compounds match the calculated tungsten trioxide percentage indicating that all compounds decomposed to WO_3 upon heating (Table 3).

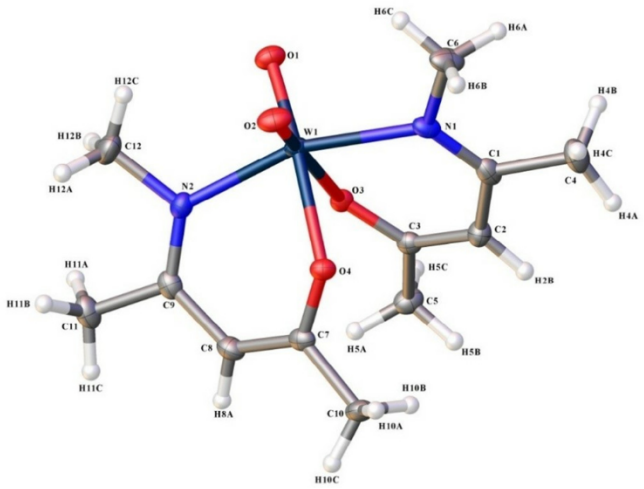

Fig. 2. Molecular structure of **2**. Thermal ellipsoids are drawn at the 50% probability level.

3.6. Mass spectrometry

The fragmentation pattern of tungsten dioxo complexes **1**–**3** was studied using direct analysis in real time mass spectrometry (DART-MS). Although the CVD process is most likely to generate neutral species instead of ions and the fragmentation pattern may vary with the ionization method, fragmentation tendencies during MS have shown correlation with decomposition pathways during CVD [38]. Major ions and their relative abundances are provided in Table 4.

The abundance of the molecular ions $[M+H]^+$ for **2** and **3** is low (3–6%) compared with that of compound **1** (24%), indicating the greater lability of **2** and **3** introduced by alkyl functionality attached to the imino nitrogen. The base peaks for all three compounds correspond to protonated ligand $[HL+H]^+$. In the cases of the less bulky ketoiminate complexes **1** and **2**, a small amount of $[M+HL+H]^+$ was detected. For compound **3**, the ligand apparently loses the ethyl substituent at the nitrogen atom to give rise to a small quantity of $[HL-Et]^+$ (9%). The formation of $[HL-Et]^+$ matches the previous observation that a large alkylimino group can induce facile fragmentation. Though $[M-L]^+$ was not directly observed, the dinuclear ion $[M+(M-L)]^+$, which can be formed by the reaction of $[M-L]^+$ and the original molecule by bridging of oxo groups, was detected for **1** and **2**. Analogous dimeric species $[M+(M+H)]^+$ were also observed for **1** and **2**. The absence of these dinucluear species for **3** is probably due to higher fragility or larger steric hindrance introduced by relatively large ketoiminate ligands. The presence of ligand species and $[M+(M-L)]^+$ suggests a possible decomposition pathway by protonation of one ketoiminate ligand and subsequent loss of HL, consistent with the thermolysis study.

3.7. Thermolysis study

The complex **2** was heated in an airtight vial and the gaseous byproducts were analyzed using GC–MS. Major fragments and

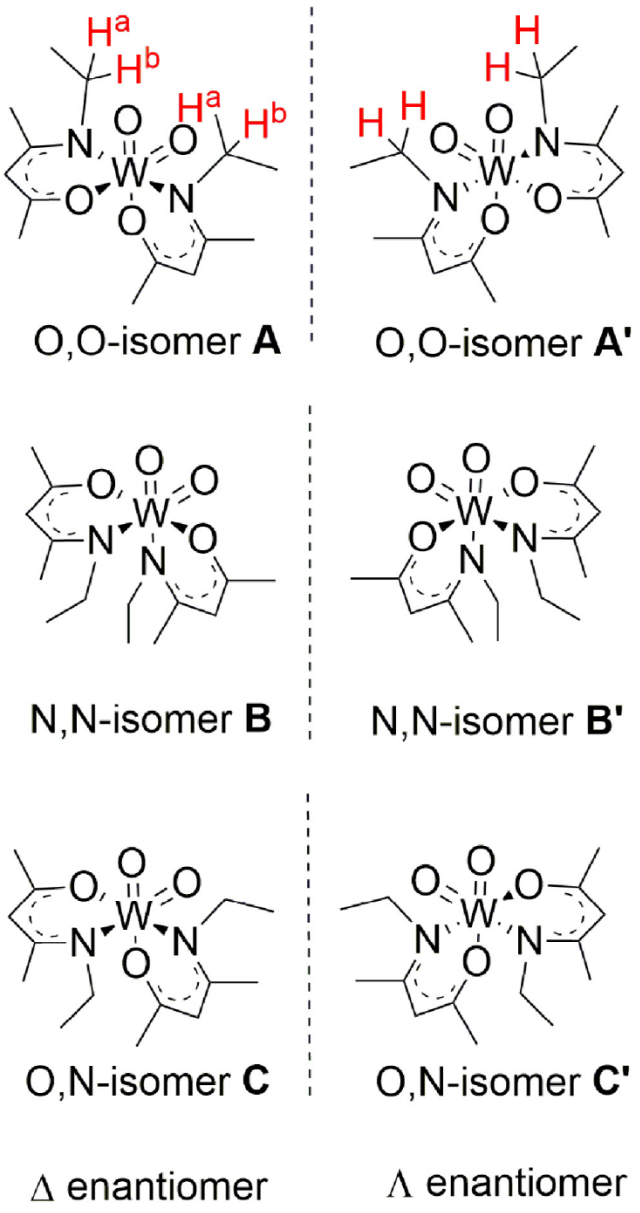

Fig. 3. Possible isomeric enantiomer pairs of WO_2L_2.

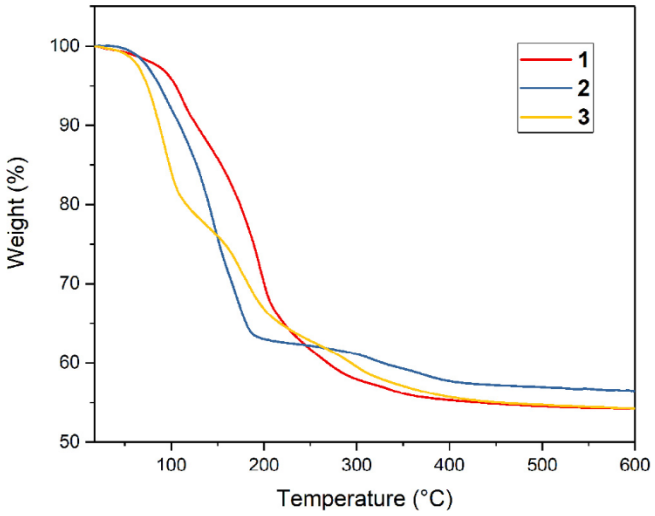

Fig. 4. Thermogravimetric analysis plots for compounds **1**–**3**.

Table 3
Experimental residual mass and the calculated WO_3 percentage for compounds **1**–**3**.

	Residual mass (%)	Calculated residual mass for WO_3 (%)
$WO_2(acNac)_2$ (**1**)	54	56
$WO_2(acNac^{Me})_2$ (**2**)	56	53
$WO_2(acNac^{iPr})_2$ (**3**)	54	50

their normalized abundance are summarized in Figs. 2–10a. The major decomposition byproducts detected by GC–MS are the protonated chelating ligand HL, N-methylpropan-2-imine and acetone. Pyrolysis of $acNac^{Me}H$ under the same conditions generated acetone as the dominant decomposition product. The presence of HL suggests a decomposition pathway in which one ketoiminate is protonated by an adjacent proton and then HL dissociates to generate intermediate **4** (Fig. 5b). The small quantities of other fragments could be products of subsequent reactions of the ketoimine and N-methylpropan-2-imine such as hydrolysis and further decomposition.

3.8. Characterization of WO_x films

Complex **2** was utilized as a precursor to grow tungsten oxide films on native silicon dioxide (Si/SiO_2, n-type, (100) by AACVD at 250, 350, 450, and 530 °C respectively. Aerosol of precursor solution in diglyme was generated by a nebulizer and was then transferred into the AACVD reaction chamber by a nitrogen flow. The color of the as-deposited films from **2** varies with deposition temperature: purple (250 °C), purple and yellow (350 °C), and hazy black (450 and 530 °C).

Fig. 6 shows the plane-view SEM images of the as-deposited films from **2**. The morphology of these films varies considerably depending on the deposition temperature. No obvious microstructures were observed for films grown at 250 °C. As the temperature increases to 350 °C, packed nanorods with an average diameter of ~45 nm were observed. Longer and thinner nanorods oriented in random directions were grown at 450 °C. Bundled nanorods were synthesized when the growth temperature was further elevated to 530 °C. The transition of morphology from featureless films to highly textured materials as the growth temperature increases is consistent with our previous AACVD experiments using other single source precursors [13,15].

The composition of the as-deposited and sputtered films deposited from precursor **2** was characterized by X-ray photoelectron spectroscopy. The sputtering process took 2 min for each film using a 2 kV Ar^+ source. The spectra of the as-synthesized films were calibrated using the adventitious C 1s peak at 284.8 eV. For the sputtered films, the C 1s spectra had a low signal to noise ratio, thus the O 1s peak at 530.5 eV which corresponds to tungsten-bonded oxygen was used as reference [13,15]. The atomic percentage of W, O, C, and N as well as the O:W ratio are reported in Fig. 7. A small amount of nitrogen was detected before (<6 at%) and after sputtering (<4 at%). The binding energy (BE) of N 1s matches the binding energy of organic nitrogen species, excluding the formation of tungsten nitride [39]. For films grown at 250 and 350 °C, the amount of carbon impurities was decreased after Ar^+ bombardment, while the atomic percentage of carbon (~60%) did not change appreciably for films grown at 450 and 530 °C, indicating substantial carbon incorporation during deposition at high temperatures. The carbon contamination could arise from both solvent and ligand decomposition [40]. For the β-ketoiminate ligands

Table 4
Selected fragments observed in positive ion DART mass spectra of **1–3**.

$WO(OR)_3L$	$[M+H]^+$ *m/z* (%)	$[M+M-L]^+$ *m/z* (%)	$[M+M+H]^+$ *m/z* (%)	$[HL+H]^+$ *m/z* (%)	$[M+HL+H]^+$ *m/z* (%)
1	413.0 (24)	726.0 (30)	825.1 (3)	100.0 (100)	512.2 (5)
2	441.1 (3)	768.1 (3)	881.2 (7)	114.1 (100)	554.1 (7)
3	469.1 (6)	n. o.[a]	n. o.[a]	128.1 (100)	n. o.[a]

[a] n. o. = not observed or trace amounts less than 1%.

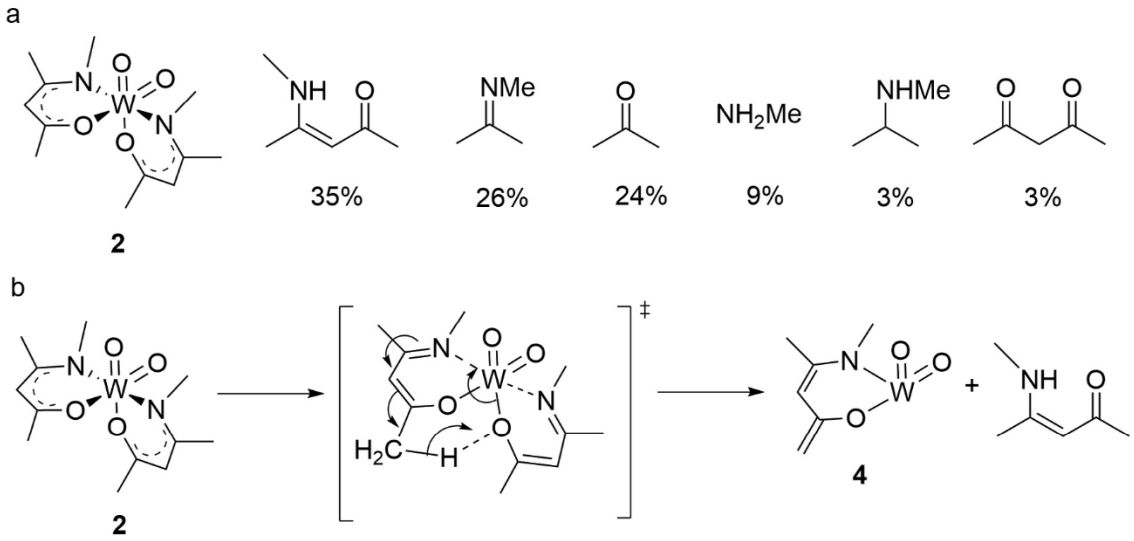

Fig. 5. (a) Thermolysis products of compounds **2**; (b) proposed decomposition mechanism.

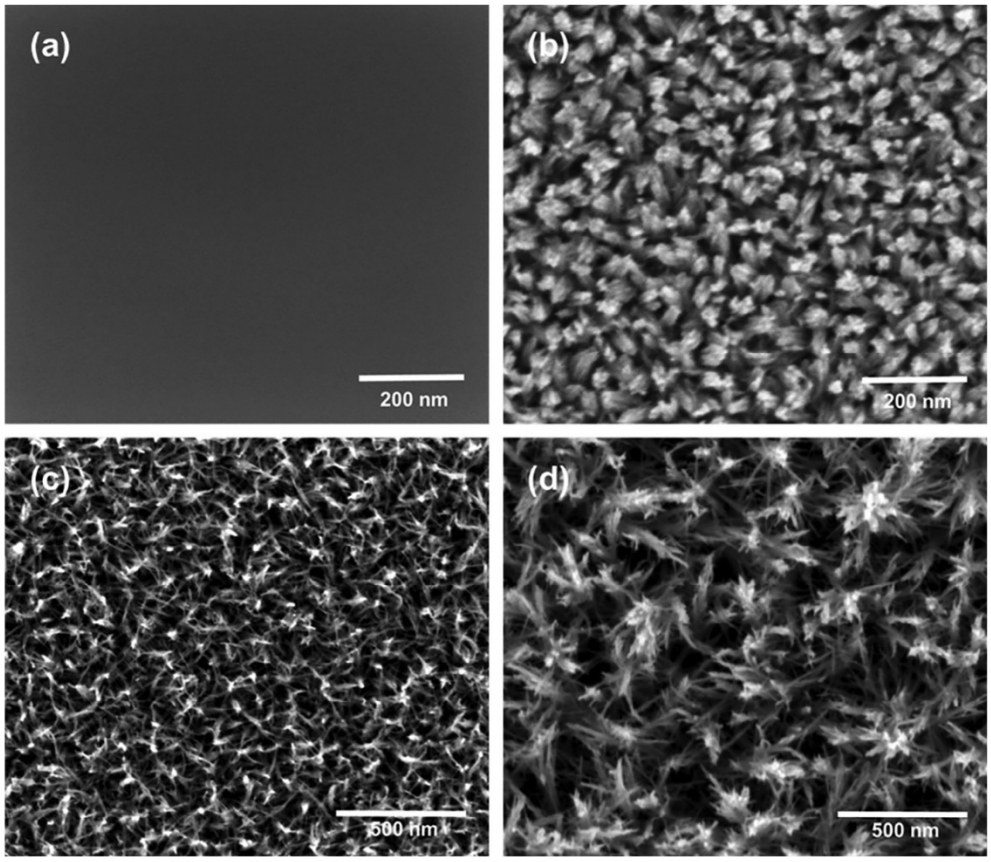

Fig. 6. Plane-view SEM images of samples grown at (a) 250, (b) 350, (c) 450 and (d) 530 °C from precursor **2** dissolved in diglyme using N_2 as carrier gas.

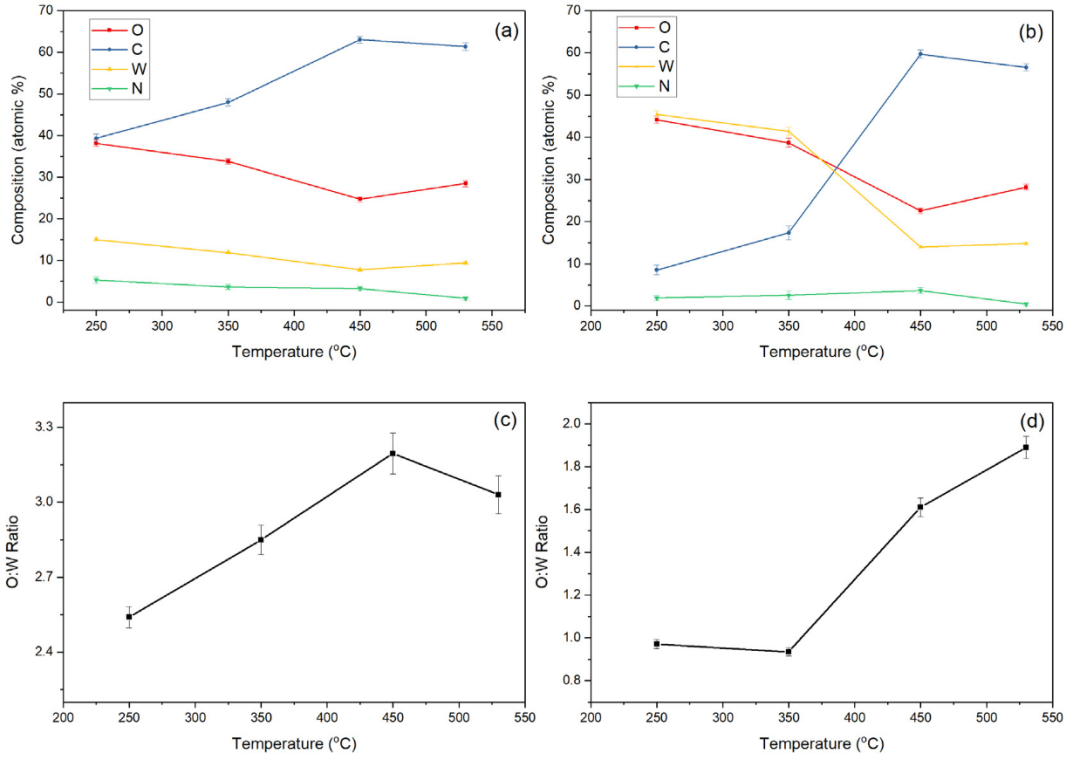

Fig. 7. XPS atomic percentage of W, O, C, and N of (a) as-synthesized films and (b) sputtered films; O:W atomic ratio of (c) as-synthesized films and (d) sputtered films grown from precursor **2**.

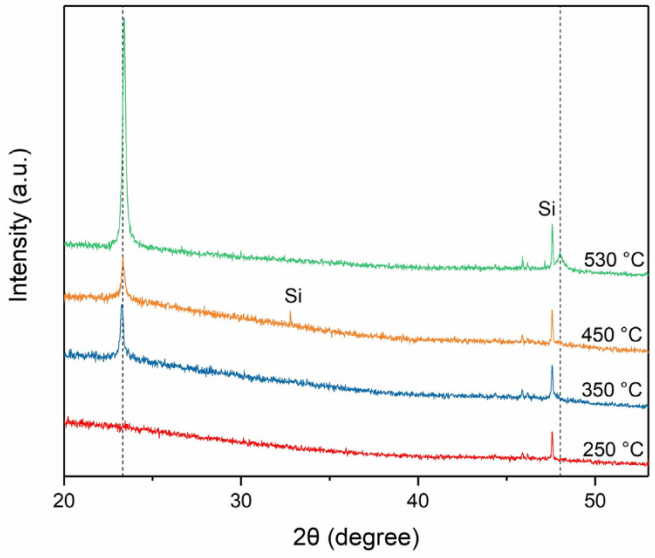

Fig. 8. XRD patterns of the as-synthesized tungsten oxide products.

which have alkyl groups attached to the nitrogen, incorporation of nitrogen content may increase the amount of carbon impurities. It has been reported that addition of water vapor during deposition process can reduce carbon impurities when using bis(diketonate) metal complexes as precursors, thus it should be possible to optimize the film composition by altering deposition conditions [41]. The O:W ratio shows a general upward trend as temperature increases. The O:W ratio of sputtered films was significantly lower than the corresponding value before sputtering. It has been reported that the ion beam bombardment of tungsten oxide can cause surface reduction by preferential removal of oxygen [42].

High resolution O 1s, C 1s and W 4f spectra of the as-grown films were analyzed to further study the chemical nature of the deposits (Fig. S1). Major carbon impurities are identified as amorphous carbon and organic C—O (285.9 ± 0.3 eV). Traces of C═O (289.0 ± 0.4 eV) were detected for films grown at 350 and 450 °C. Deconvolution of O 1s peaks confirms that oxygen is bonded to either carbon or tungsten. The XPS spectra of the W4f core levels were fitted into two sets of doublets with spin–orbit separation of 2.18 eV through the full range of deposition temperature. The BE of W $4f_{7/2}$ at 35.7 ± 0.2 eV and 34.5 ± 0.4 eV are assigned to W^{6+} and W^{5+} respectively. The amount of W^{6+} increased as the growth temperature changed from 250 to 450 °C. Deconvolution of O 1s spectra of the sputtered materials shows that C═O was removed effectively. Compared with the presence of only W^{6+} and W^{5+} in non-sputtered films, the films after Ar^+ bombardment contained tungsten in lower oxidation states such as W^{4+} and W^0 (Fig. S2). This observation is consistent with the reduction of tungsten oxides upon sputtering caused by the preferential removal of oxygen [42]. Sputtering is a complicated process which results in both chemical and morphological change of the material. The tendency towards the preferential removal of certain elements can be influenced by sputtering parameters as well as the composition, microstructure and surface topography of the films. Therefore, caution needs to be exercised when conducting depth profiling of reducible transition metal oxides such as tungsten oxides.

The crystallinity and phase of the as-synthesized deposits were studied by X-ray diffraction (XRD) analysis (Fig. 8). Films grown at 250 °C were amorphous, exhibiting only a peak for the silicon substrate. In contrast, the materials synthesized at 350–530 °C show a strong diffraction peak at 23.3° 2θ which is assigned to the (0 1 0) plane of monoclinic WO_3. The films grown at 550 °C also have a diffraction peak at 48.0° 2θ, which is indexed to the (0 4 0) facet of monoclinic WO_3 (ICCD card number 72-0677).

4. Conclusion

In summary, the bis(β-ketoiminate) dioxo tungsten(VI) complexes WO_2L_2 (L = acNac, $acNac^{Me}$, $acNac^{Et}$) have been synthesized as potential precursors for the growth of tungsten oxide films by AACVD. The results of MS and thermolysis studies were used in proposing possible thermal decomposition mechanisms for the complexes. The proton transfer steps in this mechanism suggest that a readily available source of protons during deposition may facilitate the decomposition process of the compounds containing chelating ligands. Growth of tungsten oxide from $WO_2(acNac^{Me})_2$ (**2**) by AACVD resulted in amorphous films at 250 °C, while nanorods were obtained at higher deposition temperatures. The films were contaminated by a significant amount of carbon, which we attribute to decomposition of the N-alkyl substituents of the acNac ligands. The application of non-N-alkylated acNac ligands may reduce carbon contamination. Sputtering with Ar^+ removed surface contaminants, but also reduced the tungsten oxides. XRD analysis indicates the presence of monoclinic WO_3 for materials grown at 350–530 °C.

Acknowledgements

Mass spectrometry was performed at the Mass Spectrometry Research and Education Center at University of Florida, supported by grant NIH S10 OD021758-01A1. We thank Hang Lu, Will Carden and Taehoon Kim for their assistance with materials characterization.

Appendix A. Supplementary data

Supplementary data to this article can be found online at https://doi.org/10.1016/j.poly.2019.05.013.

References

[1] C.G. Granqvist, Electrochromics for smart windows: Oxide-based thin films and devices, Thin Solid Films 564 (2014) 1.
[2] C.G. Granqvist, Electrochromic tungsten oxide films: review of progress 1993–1998, Sol. Energy Mater. Sol. Cells 60 (2000) 201.
[3] M. Vasilopoulou, G. Papadimitropoulos, L.C. Palilis, D.G. Georgiadou, P. Argitis, S. Kennou, I. Kostis, N. Vourdas, N.A. Stathopoulos, D. Davazoglou, High performance organic light emitting diodes using substoichiometric tungsten oxide as efficient hole injection layer, Org. Electron. 13 (2012) 796.
[4] D.B. Migas, V.L. Shaposhnikov, V.E. Borisenko, Tungsten oxides. II. The metallic nature of Magnéli phases, J. Appl. Phys. 108 (2010) 093714.
[5] H.D. Zheng, J.Z. Ou, M.S. Strano, R.B. Kaner, A. Mitchell, K. Kalantar-Zadeh, Nanostructured tungsten oxide – properties, synthesis, and applications, Adv. Funct. Mater. 21 (2011) 2175.
[6] S. Cong, F. Geng, Z. Zhao, Tungsten oxide materials for optoelectronic applications, Adv. Mater. 28 (2016) 10518.
[7] A.C. Jones, M.L. Hitchman, Chemical Vapor Deposition: Precursors, Processes and Applications, RSC Publishing, 2009.
[8] U. Riaz, Low-temperature atmospheric-pressure chemical vapor deposition of tungsten oxide thin films, Thin Solid Films 235 (1993) 15.
[9] C.S. Blackman, X. Correig, V. Katko, A. Mozalev, I.P. Parkin, R. Alcubilla, T. Trifonov, Templated growth of tungsten oxide micro/nanostructures using aerosol assisted chemical vapour deposition, Mater. Lett. 62 (2008) 4582.
[10] C.Y. Xu, M.J. Hampden-Smith, T.T. Kodas, Aerosol-assisted chemical-vapor-deposition (AACVD) of binary alloy (Ag_xPd_{1-x}, Cu_xPd_{1-x}, Ag_xCu_{1-x}) films and studies of their compositional variation, Chem. Mater. 7 (1995) 1539.
[11] W.B. Cross, I.P. Parkin, S.A. O'Neill, P.A. Williams, M.F. Mahon, K.C. Molloy, Tungsten oxide coatings from the aerosol-assisted chemical vapor deposition of $W(OAr)_6$ (Ar = C_6H_5, C_6H_4F-4, $C_6H_3F_2$-3,4); photocatalytically active γ-WO_3 films, Chem. Mater. 15 (2003) 2786.
[12] R.O. Bonsu, D.C. Bock, H. Kim, R.Y. Korotkov, K.A. Abboud, T.J. Anderson, L. McElwee-White, Synthesis and evaluation of κ^2-β-diketonate and β-ketoesterate tungsten(VI) oxo-alkoxide complexes as precursors for chemical vapor deposition of WO_x thin films, Dalton Trans. 45 (2016) 10897.
[13] D.C. Bock, N.C. Ou, R.O. Bonsu, C.T. Anghel, X. Su, L. McElwee-White, Synthesis of tungsten oxo fluoroalkoxide complexes $WO(OR)_3L$ as precursors for growth of WO_x nanomaterials by aerosol-assisted chemical vapor deposition, Solid State Ionics 315 (2018) 77.
[14] G.V. Kunte, S.A. Shivashankar, A.M. Umarji, Thermal analysis and vapor pressure of a new series of tungsten(VI) oxo-alkoxide-β-ketoesterate complex precursors for the chemical vapour deposition of tungsten oxide, Thermochim Acta 474 (2008) 12.
[15] X. Su, T. Kim, K.A. Abboud, L. McElwee-White, Synthesis of β-ketoiminate and β-iminoesterate tungsten (VI) oxo-alkoxide complexes as AACVD precursors for growth of WO_x thin films, Polyhedron 157 (2019) 548.
[16] R.O. Bonsu, H. Kim, C. O'Donohue, R.Y. Korotkov, K.A. Abboud, T.J. Anderson, L. McElwee-White, Dioxo-fluoroalkoxide tungsten(VI) complexes for growth of WO_x thin films by aerosol-assisted chemical vapor deposition, Inorg. Chem. 54 (2015) 7536.
[17] K.C. Molloy, P.A. Williams, Atmospheric pressure chemical vapor deposition of WO_3 thin films from a volatile fluorinated tungsten oxo-alkoxide precursor, $W(O)(OCH_2CF_3)_4$, Appl. Organomet. Chem. 22 (2008) 560.
[18] D.V. Baxter, M.H. Chisholm, S. Doherty, N.E. Gruhn, Chemical vapour deposition of electrochromic tungsten oxide films employing volatile tungsten(VI) oxo alkoxide/β-diketonate complexes, Chem. Commun. (1996) 1129.
[19] H.J. Wengrovius, R.R. Schrock, Synthesis and characterization of tungsten oxo neopentylidene complexes, Organometallics 1 (1982) 148.
[20] K. Dreisch, C. Andersson, C. Staalhandske, Synthesis and structure of dimethoxyethanedichlorodioxotungsten(VI)-a highly soluble derivative of tungsten dioxodichloride, Polyhedron 10 (1991) 2417.
[21] M. Litvic, M. Filipan, I. Pogorelic, I. Cepanec, Ammonium carbamate; mild, selective and efficient ammonia source for preparation of β-amino-α, β-unsaturated esters at room temperature, Green Chem. 7 (2005) 771.
[22] F. Strube, S. Rath, J. Mattay, Functionalized fulgides and fluorophore-photoswitch conjugates, Eur. J. Org. Chem. (2011) 4645.
[23] A.V. Korolev, V.R. Pallem, Synthesis of Copper(II) Complexes with Diketiminate and Ketoiminate, American Air Liquide, Inc., US, 2014, Patent US8692010B.
[24] K.R. McClain, C. O'Donohue, Z. Shi, A.V. Walker, K.A. Abboud, T. Anderson, L. McElwee-White, Synthesis of $WN(NMe_2)_3$ as a precursor for the deposition of WN_x nanospheres, Eur. J. Inorg. Chem. (2012) 4579–4584.
[25] H. Kim, R.O. Bonsu, D.C. Bock, N.C. Ou, R.Y. Korotkov, L. McElwee-White, T.J. Anderson, Tungsten oxide film and nanorods grown by aerosol-assisted chemical vapor deposition using κ^2-β-diketonate and β-ketoesterate tungsten(VI) oxo-alkoxide precursors, ECS J. Solid State Sci. Technol. 5 (2016) Q3095.
[26] G.M. Sheldrick, Crystal structure refinement with SHELXL, Acta Crystallogr., Sect. C 71 (2015) 3.
[27] P.J. Wright, M.J. Crosbie, P.A. Lane, D.J. Williams, A.C. Jones, T.J. Leedham, H.O. Davies, Metal organic chemical vapor deposition (MOCVD) of oxides and ferroelectric materials, J. Mater. Sci.-Mater. Electron. 13 (2002) 671.
[28] G.E. Buono-Core, A.H. Klahn, C. Castillo, M.J. Bustamante, E. Munoz, G. Cabello, B. Chornik, Synthesis and evaluation of bis-β-diketonate dioxotungsten(VI) complexes as precursors for the photodeposition of WO_3 films, Polyhedron 30 (2011) 201.
[29] A.R. Mouat, A.U. Mane, J.W. Elam, M. Delferro, T.J. Marks, P.C. Stair, Volatile hexavalent oxo-amidinate complexes: molybdenum and tungsten precursors for atomic layer deposition, Chem. Mater. 28 (2016) 1907.
[30] G. Lyashenko, G. Saischek, M.E. Judmaier, M. Volpe, J. Baumgartner, F. Belaj, V. Jancik, R. Herbst-Irmer, N.C. Mosch-Zanetti, Oxo-molybdenum and oxo-tungsten complexes of Schiff bases relevant to molybdoenzymes, Dalton Trans. (2009) 5655.
[31] Z. Liu, H.X. Chen, D. Huang, Y. Zhang, Y.M. Yao, A facile route to lithium complexes supported by β-ketoiminate ligands and their reactivity, J. Organomet. Chem. 749 (2014) 7.
[32] V. Vrdoljak, J. Pisk, B. Prugovecki, D. Agustin, P. Novak, D. Matkovic-Calogovic, Dioxotungsten(VI) complexes with isoniazid-related hydrazones as (pre)catalysts for olefin epoxidation: solvent and ligand substituent effects, RSC Adv.. 6 (2016) 36384.
[33] Y.L. Wong, L.H. Tong, J.R. Dilworth, D.K.P. Ng, H.K. Lee, New dioxo-molybdenum(VI) and -tungsten(VI) complexes with N-capped tripodal N_2O_2 tetradentate ligands: synthesis, structures and catalytic activities towards olefin epoxidation, Dalton Trans. 39 (2010) 4602.
[34] D.C. Brower, J.L. Templeton, D.M.P. Mingos, Metal dπ-ligand π-conflicts in octahedral oxo, carbyne, and carbonyl-complexes, J. Am. Chem. Soc. 109 (1987) 5203.
[35] R.J. Butcher, B.R. Penfold, E. Sinn, Crystal-structures of cis-dibromodioxobis (triphenylphosphine oxide) molybdenum(VI), cis-dichlorodioxobis (triphenylphosphine oxide)molybdenum(VI), and cis-bis(butane-2,3-diolato)dioxomolybdenum(VI)-butane-2,3-diol (1–2) – comparison of coordination spheres and the general stereochemistry of molybdenum(VI) Oxo-Complexes, J. Chem. Soc., Dalton Trans. (1979) 668.
[36] M.E. Judmaier, C. Holzer, M. Volpe, N.C. Mosch-Zanetti, Molybdenum(VI) dioxo complexes employing Schiff base ligands with an intramolecular donor for highly selective olefin epoxidation, Inorg. Chem. 51 (2012) 9956.
[37] Q.L. Xia, Y. Cui, D. Yuan, Y.R. Wang, Y.M. Yao, Synthesis and characterization of lanthanide complexes stabilized by N-aryl substituted β-ketoiminato ligands and their application in the polymerization of rac-lactide, J. Organomet. Chem. 846 (2017) 161.
[38] O.J. Bchir, K.M. Green, H.M. Ajmera, E.A. Zapp, T.J. Anderson, B.C. Brooks, L.L. Reitfort, D.H. Powell, K.A. Abboud, L. McElwee-White, The tungsten allylimido complexes $Cl_4(RCN)W(NC_3H_5)$ as single-source CVD precursors for WN_xC_y thin films. correlation of precursor fragmentation to film properties, J. Am. Chem. Soc. 127 (2005) 7825.

[39] A. Mohtasebi, T. Chowdhury, L.H.H. Hsu, M.C. Biesinger, P. Kruse, Interfacial charge transfer between phenyl-capped aniline tetramer films and iron oxide surfaces, J. Phys. Chem. C 120 (2016) 29248.
[40] O.J. Bchir, K.M. Green, M.S. Hlad, T.J. Anderson, B.C. Brooks, L. McElwee-White, Tungsten nitride thin films deposited by MOCVD: sources of carbon and effects on film structure and stoichiometry, J. Cryst. Growth 261 (2004) 280.
[41] T. Weiss, V. Zielasek, M. Baumer, Influence of water on chemical vapor deposition of Ni and Co thin films from ethanol solutions of acetylacetonate precursors, Sci. Rep. 5 (2015).
[42] F.Y. Xie, L. Gong, X. Liu, Y.T. Tao, W.H. Zhang, S.H. Chen, H. Meng, J. Chen, XPS studies on surface reduction of tungsten oxide nanowire film by Ar+ bombardment, J. Electron. Spectrosc. Relat. Phenom. 185 (2012) 112.